SCIENTIFIC REPORTS

OPEN

SUBJECT AREAS:
METALS AND ALLOYS
GLASSES
COMPOSITES

Received
26 September 2013

Accepted
11 November 2013

Published
27 November 2013

Correspondence and requests for materials should be addressed to Z.P.L. (luzp@ustb.edu.cn)

Designing novel bulk metallic glass composites with a high aluminum content

Z. P. Chen, J. E. Gao, Y. Wu, H. Wang, X. J. Liu & Z. P. Lu

State Key Laboratory for Advanced Metals and Materials, University of Science and Technology Beijing, Beijing 100083, China.

The long-standing challenge for forming Al-based BMGs and their matrix composites with a critical size larger than 1 mm have not been answered over the past three decades. In this paper, we reported formation of a series of BMG matrix composites which contain a high Al content up to 55 at.%. These composites can be cast at extraordinarily low cooling rates, compatible with maximum rod diameters of over a centimetre in copper mold casting. Our results indicate that proper additions of transition element Fe which have a positive heat of mixing with the main constituents La and Ce can appreciably improve the formability of the BMG matrix composites by suppressing the precipitation of Al(La,Ce) phase resulted from occurrence of the phase separation. However, the optimum content of Fe addition is strongly dependant on the total amount of the Al content in the Al-(CoCu)-(La,Ce) alloys.

Bulk metallic glasses (BMGs) constitute a new class of metallic materials which usually show superior properties to their crystalline counterparts[1–9], such as high specific strength, high hardness and large elastic limit. In particular, Al-based based metallic glasses have a lower density and higher specific strength compared to other metal-based metallic glasses[10], which makes them viable for aerospace industrial applications[11–13]. Therefore, serious research efforts have been devoted to developing novel light-weight Al-based BMGs[14–18] ever since the first Al-based metallic glass ribbon was discovered in 1988[6]. Up to date, however, material scientists and physicists have not yet to answer the challenge of forming Al-based BMGs that are larger than 1 mm in the smallest dimension. The formation of Al-based metallic glasses and their composites is limited to thin ribbons which seriously restrict their widespread applications as engineering materials[10].

Numerous studies indicated that glass-forming ability (GFA) of Al-based alloy systems cannot be readily understood by currently available wisdoms[19–26], such as the confusion principle[27], Inoue's empirical criterion[3], GFA indicators (i.e., reduced glass transition temperature[28], supercooled liquid range[3], and γ parameter[29,30], which gives rise to difficulty in exploring Al-based BMGs with enhanced GFA. As such, researchers have attempted to produce bulk amorphous Al-based alloys and their composites with powder metallurgy methods by consolidating their glassy ribbons or powders[31–33]. Nevertheless, this kind of processes is costly and the mechanical properties of the produced materials are severely degraded due to formation of defects and voids[3,31–33]. In this paper, we report formation of a series of BMG matrix composites which containing a high Al content from 35 to 60 at.%. In addition, it was found that additions of Fe, which has a positive heat of mixing with the main constitute elements La and Ce, further enhanced the volume fraction of glass matrix by suppressing the precipitation of the Al(La,Ce) phase.

Results

Formation of BMG matrix composites in the Al-(Co,Cu)-(La,Ce) alloy system. Figure 1a shows the maximum attainable rod diameter of BMG matrix composites as a function of chemical composition in the Al-(Co,Cu)-(La,Ce) alloy system. In our study, we defined the BMG matrix composite which contains at least a volume fraction of 20% glass phase. For the alloys containing a Al content ranging from 5 to 30 at.%, fully glassy rods can be produced, as shown in the shadowed region in Fig. 1a. In particular, the maximum attainable rod diameter for fully glass formation is 32 mm[34] for the alloys containing 10 at.% Al. It was reported that the increment in Al drastically reduces the glass forming ability in this alloy system. As the content of Al is increased to 30 at.%, the maximum attainable rod diameter of fully glass is dramatically decreased to 2 mm[35]. For the alloys containing a high Al content (i.e., 45–55 at.%), fully glassy rods can no longer be produced by conventional copper mold casting[36].

However, our experimental data showed that BMG matrix composites with homogeneously distributed crystalline phases in the high Al range could be still formed by carefully adjusting the relative concentration of the

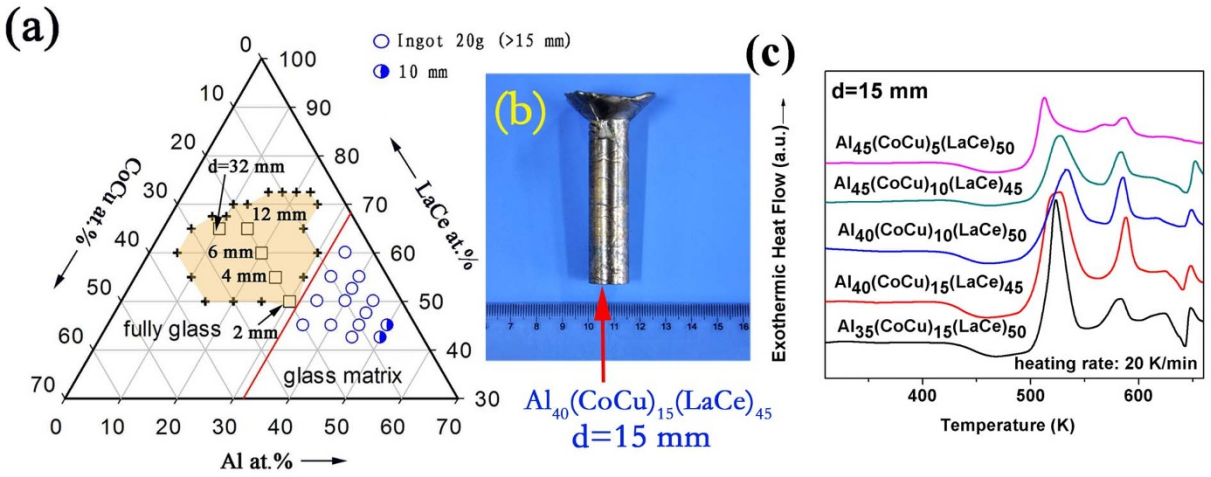

Figure 1 | (a)The critical thickness for BMG matrix composites as a function of alloy compositions, and (b) outer appearance of the as-cast $Al_{40}(CoCu)_{15}C(LaCe)_{45}$ BMG matrix composites with a diameter of 15 mm, and (c) DSC curves of the rods with a diameter of 15 mm for the $Al_{35}(CoCu)_{15}C(LaCe)_{50}$, $Al_{40}(CoCu)_{15}C(LaCe)_{45}$, $Al_{40}(CoCu)_{10}C(LaCe)_{50}$, $Al_{45}(CoCu)_{10}C(LaCe)_{45}$ and $Al_{45}(CoCu)_5C(LaCe)_{50}$ alloys.

constituents in the alloy system. For the alloys containing less than 45 at.% Al, BMG matrix composites can be obtained directly from the as-cast ingots with a weight up to 20 g, and equivalently, the critical thickness of these BMG composites is larger than 15 mm. As an example, Figure 1b shows the outer appearance of the as-cast $Al_{40}(CoCu)_{15}(LaCe)_{45}$ alloy rod with a diameter of 15 mm, and Figure 1c shows the DSC curves of the as-cast $Al_{35}(CoCu)_{15}(LaCe)_{50}$, $Al_{40}(CoCu)_{15}(LaCe)_{45}$, $Al_{40}(CoCu)_{10}(LaCe)_{50}$, $Al_{45}(CoCu)_{10}(LaCe)_{45}$ and $Al_{45}(CoCu)_5(LaCe)_{50}$ alloy ingots with a weight of 20 g at a heating rate of 20 K/min. All the ingots clearly show a glass transition event and an exothermic crystallization behavior, implying that all these as-cast ingots have an amorphous matrix. Furthermore, all samples have a similar glass transition temperature (T_g) and onset crystallization temperature (T_x), indicating that the amorphous matrix have a similar chemical composition. As the Al content increases to 50 at.%, the maximum attainable rod diameter is decreased to about 10 mm. With the further increase of the Al content to 55 at.%, the attainable rod diameter for composite formation is dramatically reduced to only 2 mm, while glassy matrix can no longer be formed in the alloys with above 55% Al.

Phase competition during formation of the BMG matrix composites in the Al-(Co,Cu)-(La,Ce) alloy system. For the alloys containing below 35 at.% Al, their GFA is seemingly large enough even for forming BMG matrix in the as-cast ingots. To unveil phase completion during solidification of this type of alloys, Figure 2a exemplarily shows SEM image of the cross section of the as-cast $Al_{35}(CoCu)_{15}(LaCe)_{50}$ alloy rod with a diameter of 15 mm, which vividly illustrates a composite structure consisting of dark coarse dendrites embedded in the white matrix. The corresponding XRD pattern of this particular sample shown in Fig. 2b confirms that the white matrix is amorphous and the dark dendrite is the $Al_2(La,Ce)$ phase. The volume fraction of the glass matrix is estimated to be as high as 80% by analyzing the SEM image. In addition, the transition element Co and Cu were found to be exchangeable and their individual amount could be varied from 5 to 20 at.%.

For the alloys containing 40 ~ 45% Al, compositional effects on the microstructure of the BMG matrix composites started to become more complex. Figure 3 shows SEM images and the corresponding XRD patterns of the as-cast 6 mm rods for the $Al_{40}(CoCu)_x(LaCe)_{60-x}$(x = 7.5, 10 and 12.5 at.%) alloys. For the alloy containing 12.5 at.% Co and Cu, only one single $Al_2(La,Ce)$ crystalline phase precipitated in the amorphous matrix (Fig. 3a), which is similar to the morphology of the $Al_{35}(CoCu)_{15}(LaCe)_{50}$ alloy rod (Fig. 2a). As the content of Co and Cu decreased to 10 at.%, two kinds of crystalline phases, i.e., $Al_2(La,Ce)$ and Al(La,Ce) (grey contrast in Fig. 3b), were observed and the volume fraction of the amorphous matrix is obviously decreased compared with that of the alloy containing 12.5 at.% Co and Cu. When the content of Co and Cu further decreased to 7.5 at.%, the resultant composite still consisted of the same crystalline phases. However, the volume fraction of Al(La,Ce) is remarkably increased while the content of $Al_2(La,Ce)$ is decreased (Fig. 3c). These results indicates that proper content of Co and Cu can suppress the precipitation of Al(La,Ce). In addition, all the glass matrix have a similar composition of $Al_{25}(CoCu)_{15}(LaCe)_{60}$ according to the EDX analysis (not shown) and the volume fraction of the glass matrix for these three alloys is about 60, 20, 40%, respectively. Similar phase competition results have been observed in the alloys with 45 at.% Al, and formation of the glass matrix and primary phases are dependent on the total amount of Co and Cu.

Alloying effects on formation of BMG composites in the alloys with above 50 at.% Al. As mentioned earlier, BMG composites in Al-(Co,Cu)-(La,Ce) alloy system is difficult to form when the content of Al exceeds 50 at.%. In our study, it was found that additions of proper elements which have a positive heat of mixing with the rare earths (i.e., La and/or Ce) could effectively facilitate formation of BMG composites. Figure 4 shows the morphology and the corresponding XRD pattern of the as-cast 10 mm rod for the $Al_{50}(CoCu)_5(LaCe)_{45-x}Fe_x$(x = 0, 5 and 10 at.%) alloys. As can be seen, the $Al_{50}(CoCu)_5(LaCe)_{45}$ alloy with no Fe addition exhibits three different contrast regions, i.e., the dark $Al_2(La,Ce)$ phase, the grey Al(La,Ce) phase and the bright amorphous matrix (Fig. 4a), and their volume fraction is estimated to be 47, 33 and 20%, respectively. For the alloy in which the rare-earth elements were substituted by Fe, their morphology and phase formation changed appreciably, as demonstrated in Figs. 4b and c. For the alloy doped with 5 at.% Fe, i.e., $Al_{50}(CoCu)_5(LaCe)_{40}Fe_5$, formation of the grey Al(La,Ce) phase was suppressed and a small portion of the black AlFe phase and the grey needle-like Al_2Fe phase appeared instead. In addition, the volume fraction of the dark $Al_2(La,Ce)$ phase and the bright amorphous matrix is determined to be approximately 60 and 35%, respectively (Fig. 4b). With the increase of Fe, the alloy is still comprised of the black AlFe phase, the dark phase $Al_2(La,Ce)$ and the bright matrix (Fig. 4c), however, the volume fraction of the glass matrix was drastically decreased because of strong formation of AlFe and $Al_2(La,Ce)$.

In order to understand effects of the Fe substitution for La and Ce in the current Al-(Co,Cu)-(La,Ce) alloy system, DSC measurement

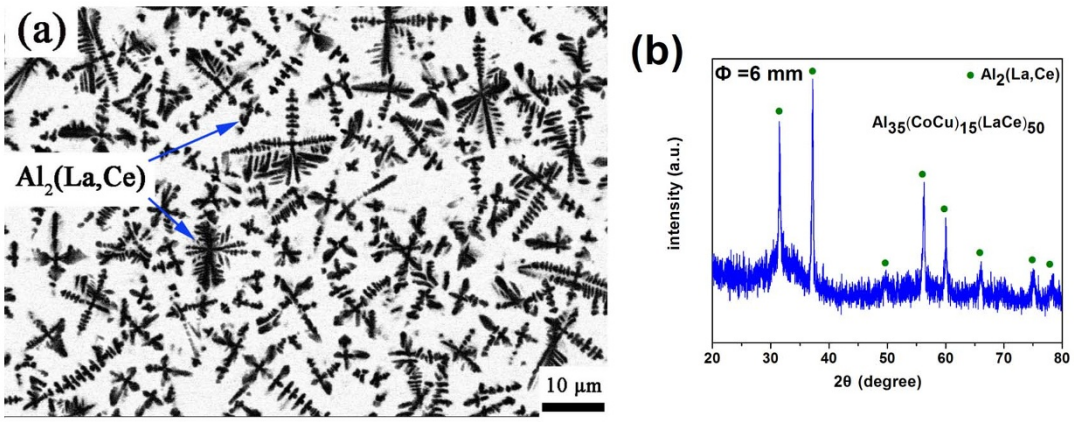

Figure 2 | **(a) SEM micrographs and the corresponding XRD pattern (b) for the as-cast alloy $Al_{35}(CoCu)_{15}C(LaCe)_{50}$ with a diameter of 10 mm.**

of the as-cast 10 mm rods for the $Al_{50}(CoCu)_5(LaCe)_{45-x}Fe_x$(x = 0, 5 and 10 at.%) alloys was also conducted at a heating rate of 20 K/min and the corresponding traces are shown in Fig. 5. For the alloys containing 50 at.% Al and with no Fe addition, the DSC trace shows a weak step change in the heat flow at a low onset temperature which corresponds to the glass transition event and a wide exothermic peak at a high onset temperature which is associated with crystallization of the amorphous matrix. When 5% Fe is added, a more distinct glass transition process and a much sharper crystallization peak were observed, implying that this alloy has a much higher volume fraction of the amorphous phase. For the alloy with 10% Fe addition, however, the DSC trace exhibits almost a straight line, suggesting that the amorphous matrix in this alloy is limited. These DSC results are consistent with the previous SEM and XRD observations in Fig. 4.

For the alloys containing 55 at.% Al, formation of BMG matrix composites became difficult. Similarly, it was found that additions of Fe could also enhance formation of the BMG matrix composites. Figure 6 shows the SEM images of the central part of the as-cast 2 mm rods for the $Al_{55}(CoCu)_5(LaCe)_{40-x}Fe_x$(x = 0, 0.5, 3 at.%) alloys. For the alloy with no Fe addition, almost no glass phase can be observed (Fig. 6a). According to the EDX analysis, the dark dendrites are Al_2(La,Ce) while the grey dendrites are Al(La,Ce). When the alloy doped with 0.5 at.% Fe, the grey Al(La,Ce) phase disappeared. The alloy mainly contains the dark Al_2(La,Ce) phase and the glass matrix with a volume fraction of 70 and 30%, respectively. HRTEM analysis (Fig. 6d) indicates that the glass matrix consists of a complete amorphous structure. However, as the Fe content increased to 3 at.%, the GFA of the matrix is reduced and the volume fraction of the bright glass matrix was decreased to 15%. Moreover, some new black crystallites which were identified as AlFe appeared (Fig. 6c). Figure 6e shows the corresponding DSC pattern for the alloys with 55% Al and different Fe concentration. For the alloy with no Fe addition, the DSC curve shows nothing but a straight line, which is consistent with the SEM observation (Fig. 6a). When 0.5 and 1 at.% Fe were added, a strong crystallization peak and a obvious glass transition process are observed, suggesting that these alloys

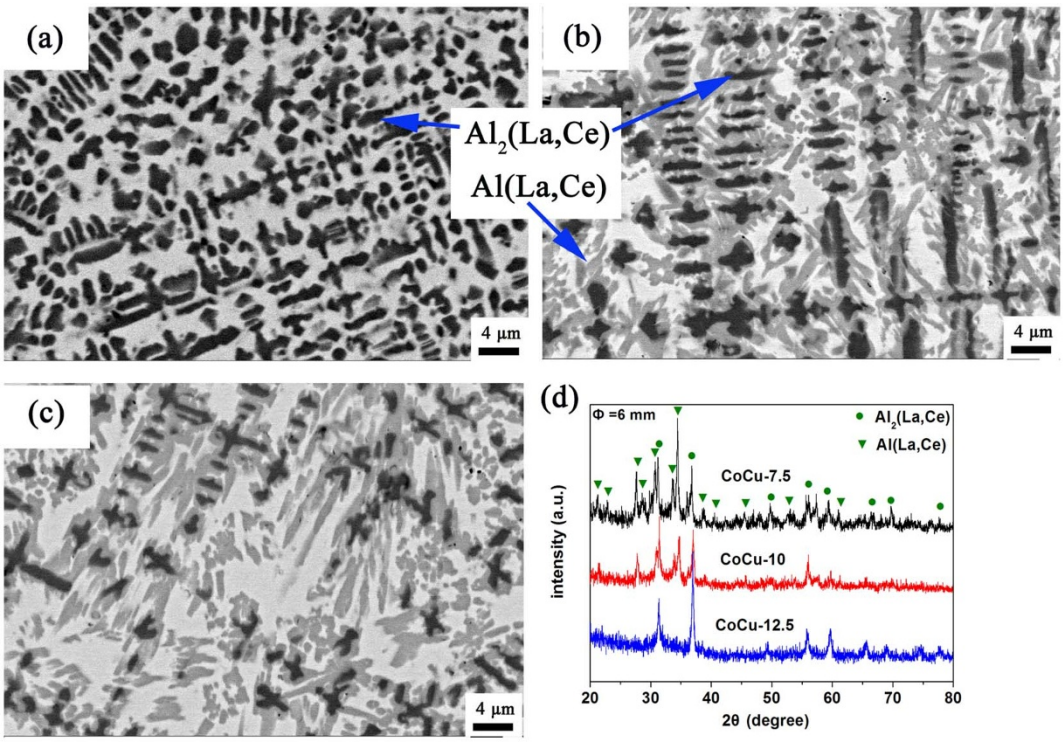

Figure 3 | SEM images for the as-cast, 6 mm rods with 40% Al; (a) $Al_{40}(CoCu)_{12.5}(LaCe)_{47.5}$, (b) $Al_{40}(CoCu)_{10}(LaCe)_{50}$, and (c) $Al_{40}(CoCu)_{7.5}(LaCe)_{52.5}$. (d) shows the corresponding XRD patterns.

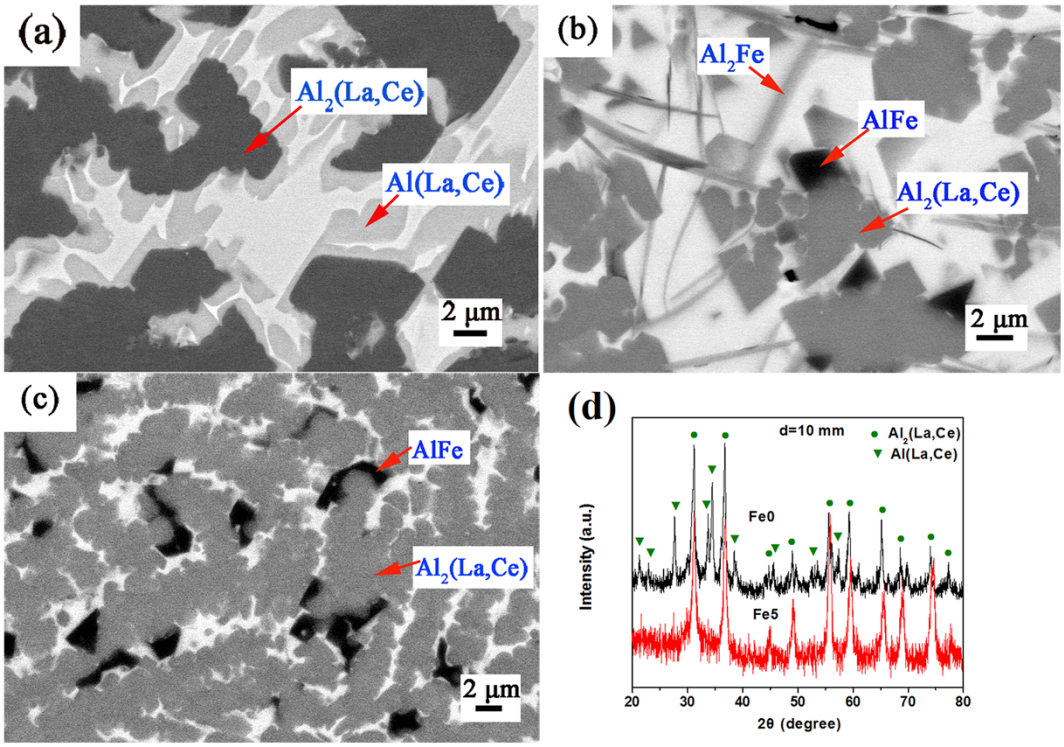

Figure 4 | SEM images for the as-cast, 10 mm rods with 50% Al; (a) $Al_{50}(CoCu)_5(LaCe)_{45}$, (b) $Al_{50}(CoCu)_5(LaCe)_{45}Fe_5$, and (c) $Al_{50}(CoCu)_5(LaCe)_{35}Fe_{10}$. (d) shows the corresponding XRD patterns.

have a much higher volume fraction of the amorphous phase. With the increase of Fe content (i.e., 3 and 5 at.%), the DSC trace became a straight line again, implying that the content of amorphous structure of these alloys are remarkably decreased. The optimal content of Fe addition is varied from 5 to 0.5 at.% as the Al content of the alloys increases from 50 to 55 at.%.

Discussion

Composition effects on formability of the BMG matrix composites in the Al-(Co,Cu)-(La,Ce) alloy system. In the Al-(Co,Cu)-(La,Ce) alloy system, the best glass formers are located at the compositions with ~10% Al, as indicated in Fig. 1a. In order to investigate the phase competition and composition effects in detail,

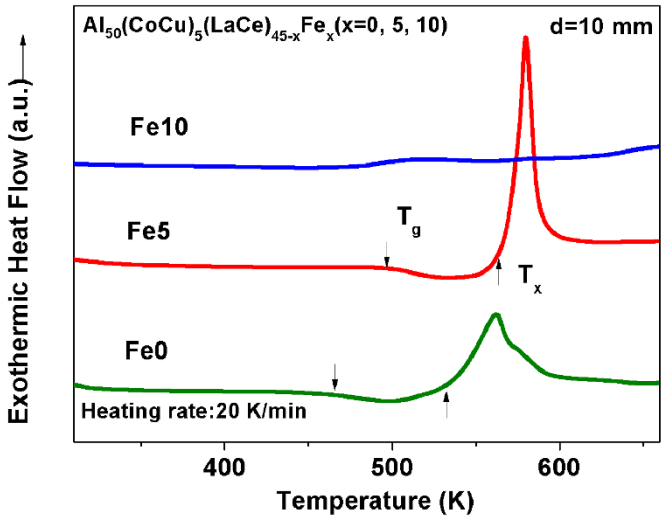

Figure 5 | DSC curves for the $Al_{50}(CoCu)_5(LaCe)_{45-x}Fe_x$(x = 0, 5, 10) alloys with a diameter of 10 mm.

melting behavior of the $Al_{50}(CoCu)_5(LaCe)_{45}$ alloy was characterized, as shown in Fig. 7. Upon heating, the alloy first exhibited an endothermic peak with an onset temperature of ~790 K, which corresponds to the melting of the originally glassy and then devitrified matrix. Subsequently, there are two more high-temperature endothermic peaks associated with the melting of the Al(La,Ce) and Al_2(La,Ce) phase, respectively. When the Al concentration was increased, the alloy composition moved away from the best glass-forming locations and formation of Al-enriched primary phases was promoted. During solidification, the primary Al-enriched phases, i.e., Al_2(La,Ce) and/or Al(La, Ce), precipitated out first from the undercooled liquid, which adjusted the composition of the remaining liquid to that of the best glass formers. Upon further cooling, the residual liquid solidified into the glass matrix, eventually leading to formation of a BMG matrix composite.

As the Al concentration is increased to 35 at.% Al, formation of the intermetallic compound Al_2(La,Ce) at high temperatures is enhanced both thermodynamically and kinetically, and the critical cooling rate for full glass formation (i.e., $R_{c\text{-}glass}$) in these alloys in determined by the TTT curve of the Al_2(La,Ce) phase, as illustrated in Fig. 8a. As a result, the GFA of these alloys is deteriorated due to the rapid formation of this compound, and the maximum attainable rod diameter of fully glassy structure is reduced to 2 mm[35]. Nevertheless, BMG matrix composites can be formed provided that the cooling rate is large enough to by-pass the nose of the eutectic TTT curve, as indicated by $R_{c\text{-}composite}$[37]. Upon cooling, the Al_2(La,Ce) phase precipitated first and the Al content in the remaining liquids decreased, and such cooling rate is sufficient to devitrify the residual liquid. In this case, BMG matrix composites normally consist of the single Al_2(La,Ce) phase embedded in the amorphous matrix.

As the Al content in the alloys is increased to 40–45 at.%, formation of the Al_2(La,Ce) phase was further promoted, resulting in an increment in the critical cooling rate and a reduction in the maximum attainable rod diameter for fully glass formation[35], as demonstrated by $R_{c\text{-}glass}$ in Fig. 8b. During cooling, the Al_2(La,Ce) phase still precipitated first, nevertheless, the remaining liquid still contained a

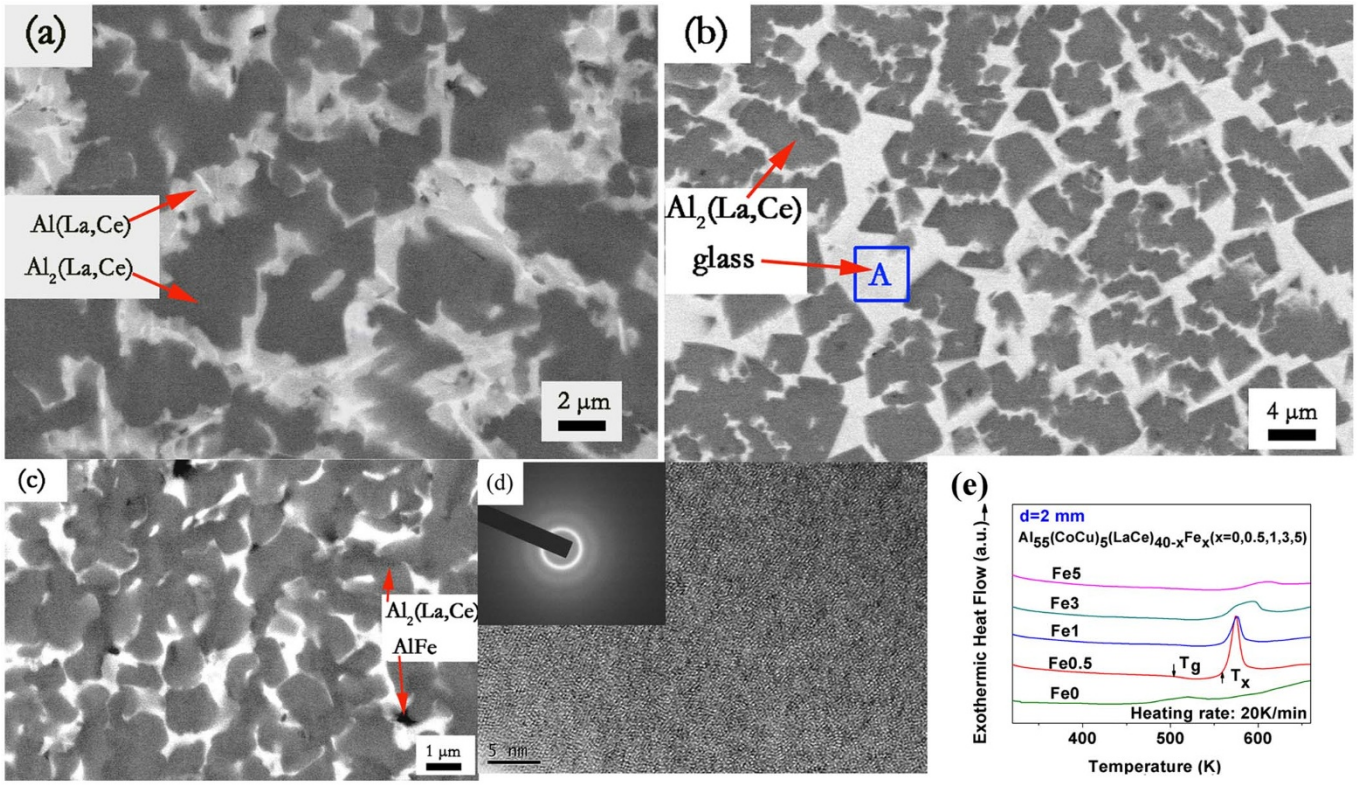

Figure 6 | SEM images for the as-cast, 2 mm rods with 55% Al; (a) $Al_{55}(CoCu)_5(LaCe)_{40}$, (b) $Al_{55}(CoCu)_5(LaCe)_{39.5}Fe_{0.5}$, and (c) $Al_{55}(CoCu)_5(LaCe)_{37}Fe_3$. (d) HRTEM image and the corresponding SAED pattern for the matrix in the $Al_{55}(CoCu)_5(LaCe)_{39.5}Fe_{0.5}$ alloy, and (e) DSC curves for all the $Al_{55}(CoCu)_5(LaCe)_{40-x}Fe_x$(x = 0, 0.5, 3) alloys.

relatively high Al content. Upon further solidification, the peritectic reaction of L′ + Al_2(La,Ce) → Al(La,Ce) tends to take place. If the alloy has a high amount of Co and Cu, such reaction would be retarded due to the necessity of long-range redistribution of these elements. As a result, in the alloys containing 40–45% Al and >7.5% (Co,Cu), BMG matrix composites, e.g., $Al_{40}(CoCu)_{12.5}(LaCe)_{47.5}$ and $Al_{45}(CoCu)_{7.5}(LaCe)_{47.5}$, still consist of the single Al_2(La,Ce) primary phase embedded in the amorphous matrix. For the alloys contain a low content of Co and Cu [e.g., $Al_{40}(CoCu)_{7.5}(LaCe)_{52.5}$ and $Al_{45}(CoCu)_5(LaCe)_{50}$], however, the peritectic reaction occurred and the second crystalline phase Al(La,Ce) appeared (see Fig. 3). Due to the high content of Al, the volume fraction of the glass matrix was reduced due to formation of more Al-enriched phases, as compared with that of the alloys having below 35% Al.

For the alloys containing above 50 at.% Al, formation of the Al_2(La,Ce) and Al(La,Ce) phases was stimulated and their TTT curves further shifted to the upper-left region (i.e., the higher-temperature and shorter-time region), as shown in Fig. 8c. As a result, the critical cooling rate for glass formation is increased rapidly. In these alloys, much more Al_2(La,Ce) phase precipitated first due to its high thermal stability. The peritectic reaction of L′ + Al_2(La,Ce) → Al(La,Ce) inevitably occurred subsequently. The volume fraction of the Al-enriched crystalline phases in these alloys was increased sharply and BMG matrix composites are hard to form.

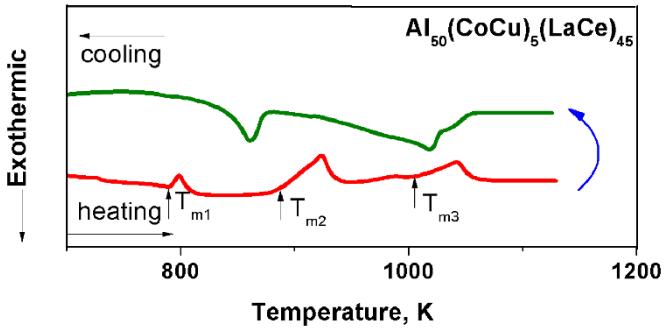

Figure 7 | **Melting and solidification curves of the $Al_{50}(CoCu)_5(LaCe)_{45}$ BMG composites at a rate of 20 K/min.**

Alloying effects of the elements with a positive heat of mixing with the rare-earths. To understand phase competition in the alloys substituted with Fe, TEM characterization of the as-cast samples for the $Al_{50}(CoCu)_5(LaCe)_{45-x}Fe_x$(x = 0, 5 at.%) alloys were conducted. The TEM image of the alloy with no Fe addition is shown in Fig. 9a, which revealed that the microstructure of this alloy consists of three different contrasts. The select area election diffraction (SAED) pattern in Fig. 9a obtained from the dark contrast was indexed as the [1 1 2] zone axis of the Al_2(La,Ce) phase, while the grey phase is Al(La,Ce) based on the SEAD pattern representing the lattice of the [1–1 2] zone axis. According to the EDX analysis, the nominal composition of these three regions was determined to be $Al_{66.5}La_{14}Ce_{19}$, $Al_{50}La_{25.5}Ce_{24.5}$ and $Al_{23}Co_7Cu_3La_{34}Ce_{33}$, respectively. Figure 9b shows the HRTEM image and the corresponding SAED of the bright matrix in Fig. 9a. As shown, the bright matrix in the as-cast $Al_{50}(CoCu)_5(LaCe)_{50}$ alloy is not fully amorphous and actually contains numerous homogenously distributed Al_2(La,Ce) nano-crystals with a size of about 2–10 nm. Comparatively, Figure 9c shows the TEM image of the alloy with 5 at.% Fe addition and the corresponding SEAD pattern, which further confirm that this particular alloy contains three different crystalline phases, i.e., Al_2(La,Ce), AlFe and Al_2Fe, along with the bright matrix. The HRTEM image and the SAED pattern of the bright matrix shown in Fig. 9d verify that a complete amorphous structure was obtained with 5% Fe addition, indicating that proper Fe addition can

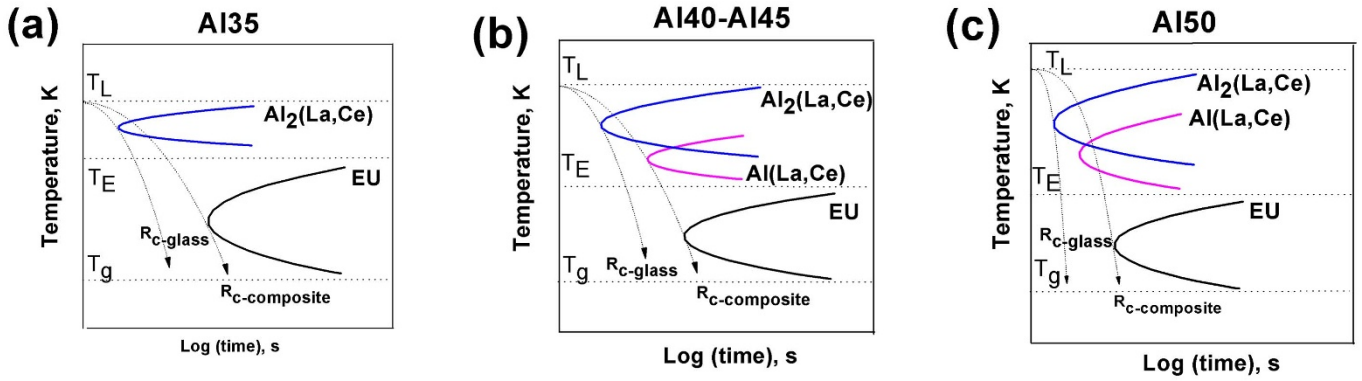

Figure 8 | **Temperature-time -transformation (TTT) curves for the Al-(CoCu)-(LaCe) alloys system containing different Al contents, schematically showing phase competition and crystallization kinetics at different undercooling; (a) 35% Al, (b)40 ~ 45% Al and (c) above 50% Al.**

effectively suppress the precipitation of the nano-Al_2(La,Ce) crystals and improve the GFA of the matrix.

To further unveil elemental partitioning during formation of the BMG matrix composites, the elemental profile in these two alloys were also characterized by the SEM line scanning analysis as shown in Fig. 10. The red arrow in Fig. 10a and c indicates the beginning and end position of the analysis. For the alloy with no Fe addition, the Al content gradually increases as the microstructure changes from the bright amorphous matrix (zone 1 in Fig. 10a) and the grey Al(La,Ce) phase (zone 2) to the dark Al_2(La,Ce) phase (zone 3). The Co and Cu elements only exist in the amorphous matrix while the La and Ce elements almost distribute uniformly in the whole sample. For the alloy contains 5 at.% Fe, the Fe element mainly exist in the grey needle-like Al_2Fe (zone 2 in Fig. 10c) and the dark Fe-rich AlFe phase (zone 4 in Fig. 10c), as can be observed in Fig. 10d which shows two maxima for the Fe element distribution in the regions 2 and 4. The enrichment of Fe always associated with the depletion of La and Ce due to the repulsion interaction between the La, Ce and Fe, and vice versa.

Based on the above observations, it can be speculated that effects of the Fe addition in the current alloy system on formation of the BMG matrix composites can originate from the composition partitioning during the solidification process. Based on the binary phase diagram of the Al-La, Al-Ce and Al-Fe systems[38], it is known that the stability of all the involved phase is in the sequence of Al_2(La,Ce), AlFe, Al_2Fe and Al(La,Ce). Figure 11 schematically illustrates the possible solidification process of the alloys containing different Fe contents. As mentioned earlier, the dark Al_2(La,Ce) phase would precipitate first

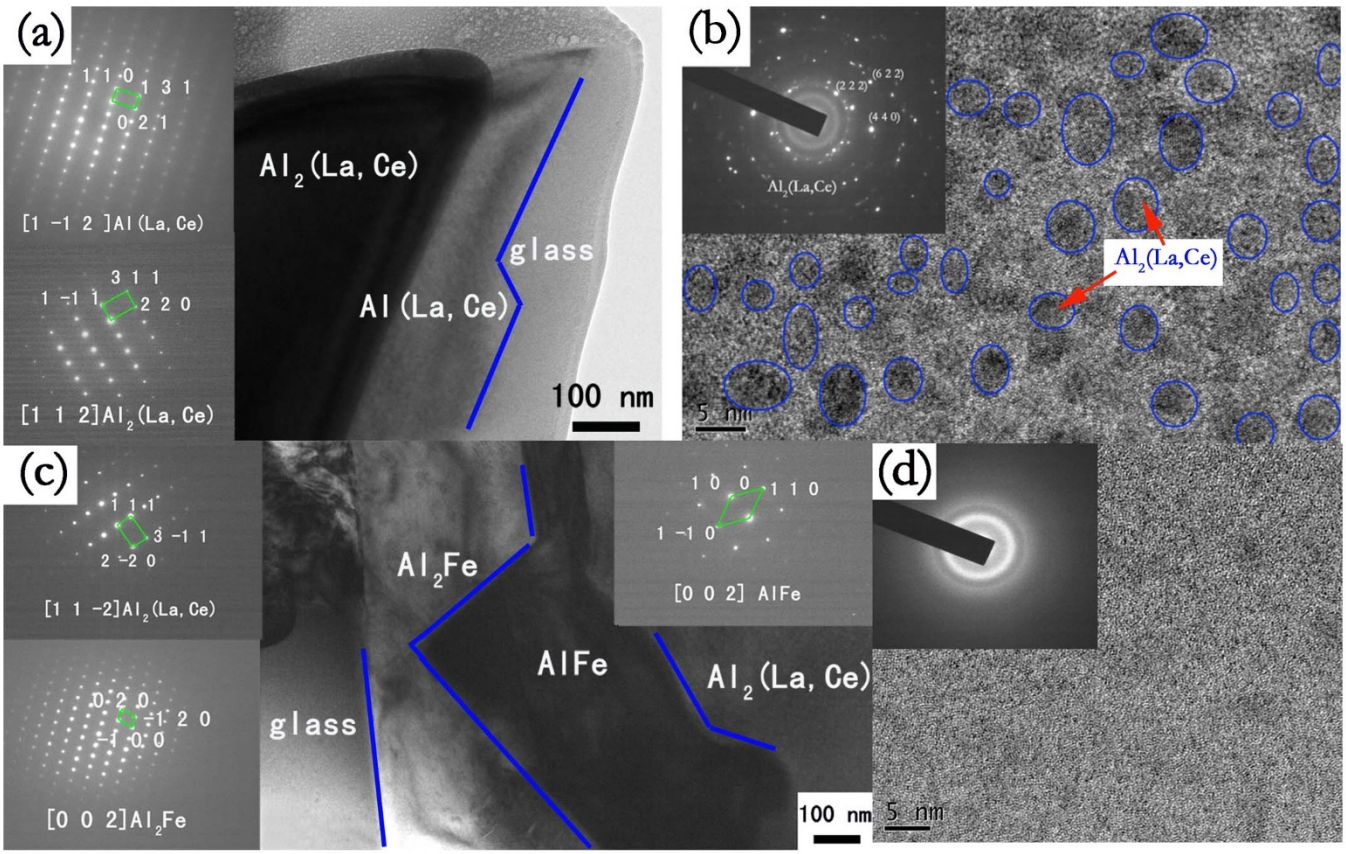

Figure 9 | TEM micrographs of the as-cast, 10 mm rods with 50% Al; (a) $Al_{50}(CoCu)_5(LaCe)_{45}$ and (c) $Al_{50}(CoCu)_5(LaCe)_{45}Fe_5$ alloys. (b) and (d) show the corresponding HRTEM images, respectively. The insets show the corresponding selected area diffraction patterns.

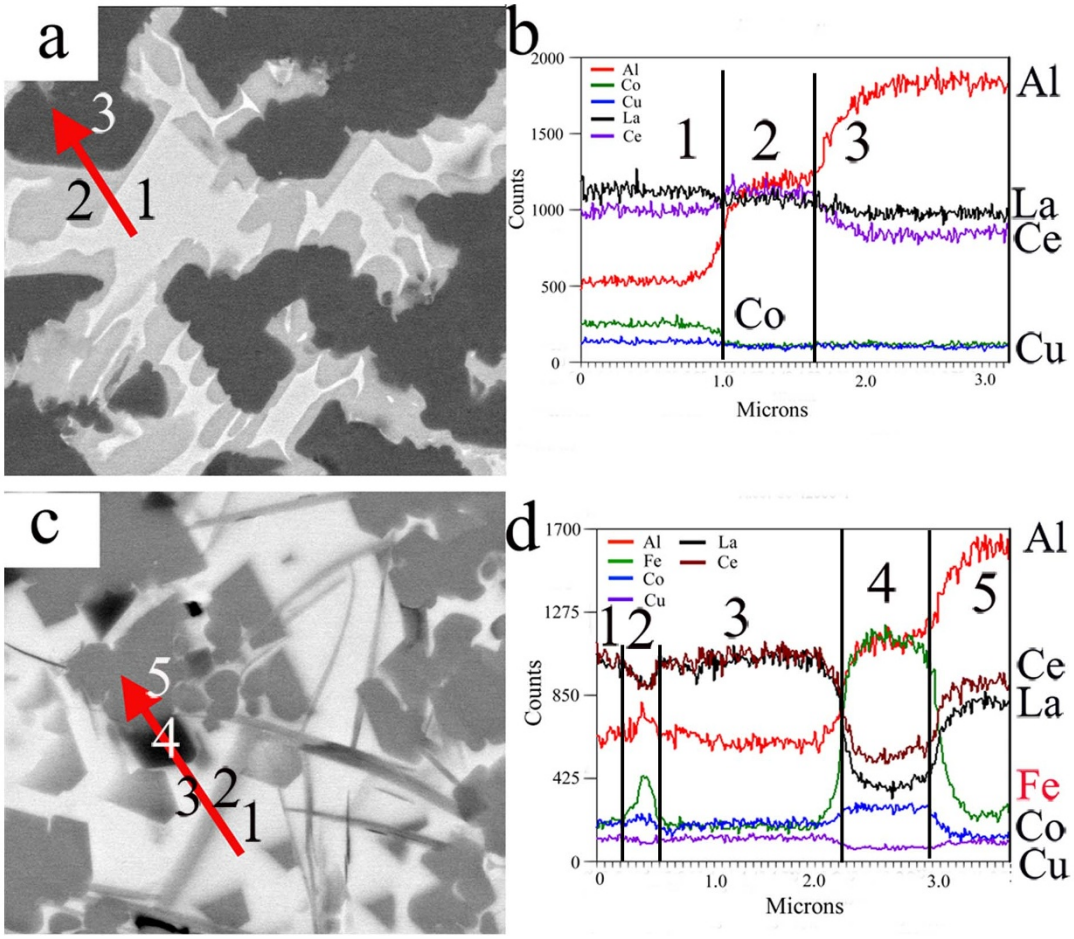

Figure 10 | **SEM line scan analysis.** Red arrows in (a) and (c) indicate the beginning and end point for the $Al_{50}Co_3Cu_2La_{22.5}Ce_{22.5}$ and $Al_{50}Co_3Cu_2La_{19}Ce_{21}Fe_5$ alloy, and (b) and (d) shows the corresponding compositional profiles.

in the alloy $Al_{50}(Co,Cu)_5(La,Ce)_{45}$ with no Fe addition, followed by the peritectic reaction of $L' + Al_2(La,Ce) \rightarrow Al(La,Ce)$. Due to the peritectic reaction, the Al content in the remaining liquid was actually increased, resulting in a reduction in the GFA. Upon further cooling, the nanosized $Al_2(La,Ce)$ crystals embedded in the amorphous matrix were obtained. For the alloy added with 5% Fe, liquid phase separation seemingly occurred, and Fe-rich and Fe-depleted liquids were formed due to the positive heat of mixing between La, Ce and Fe. During solidification, the $Al_2(La,Ce)$ phase precipitated first out of the Fe-depleted liquid, followed by formation of the needle-like AlFe and the black Al_2Fe phases from the Fe-rich liquid. Compared with that of the $Al_{50}(Co,Cu)_5(La,Ce)_{45}$ alloy, the Al content in the residual liquid of the alloy containing 5 at.% Fe is effectively reduced (i.e., adjusting the composition closer to the eutectic

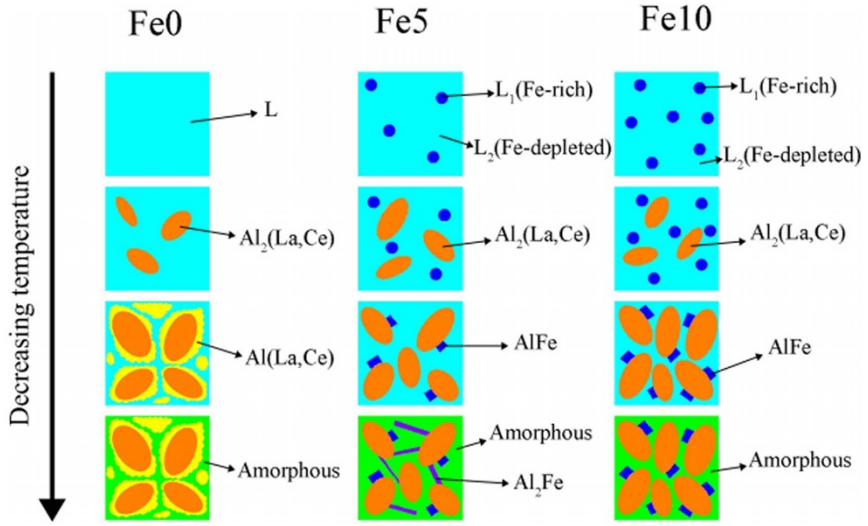

Figure 11 | **Schematic illustration of the solidification process for the $Al_{50}(CoCu)_5(LaCe)_{45-x}Fe_x$(x = 0, 5, 10) alloys.**

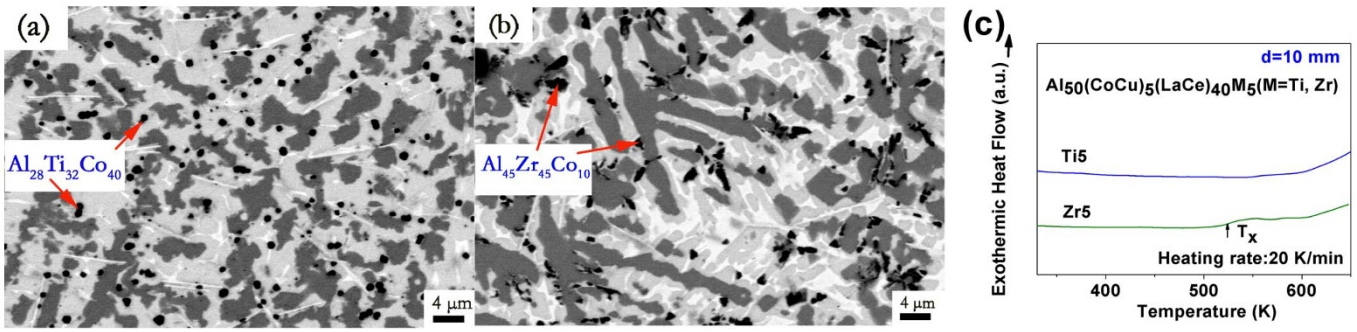

Figure 12 | SEM images for the as-cast rods added with Zr and Ti; (a) $Al_{50}(CoCu)_5(LaCe)_{40}Ti_5$ and (b) $Al_{50}(CoCu)_5(LaCe)_{40}Zr_5$. (c) shows the corresponding DSC curves.

point) due to formation of the AlFe and Al_2Fe resulted from the phase separation, leading to the enhanced GFA. For the alloy doped with 10% Fe, the liquid phase separation will also take place. Nevertheless, the volume fraction of the Fe-rich liquid is increased due to the larger amount of Fe. During cooling, the dark Al_2(La, Ce) phase still formed first from the Fe-depleted liquid. Subsequently, the AlFe phase precipitates out but without any formation of Al_2Fe because of the high Fe content. At this stage, the surplus Al in the Fe-rich liquid will be dissolved in the remain liquid, thus leading to the increase in the Al content and promoting formation of more Al_2(La, Ce) phase. Consequently, the volume fraction of the glass matrix is dramatically reduced.

Like the Fe element, both Zr and Ti also have a positive heat of mixing with La and Ce elements[39]. However, their effects on formation of the current BMG matrix composites are totally different. Figure 12 exhibits the SEM images and the corresponding DSC curves for the as-cast, 10 mm rods of the $Al_{50}(Co,Cu)_5(La,Ce)_{40}M_5$(M = Ti, Zr) alloy. For the alloy containing 5 at.% Ti, both the SEM image and DSC trace indicate that no glass matrix was obtained. According to the EDX analysis, a new primary crystalline with a composition of $Al_{28}Ti_{32}Co_{40}$ appeared (i.e., the black round phase in Fig. 12a). It seems that formation of this ternary phase induced by the addition of Ti consumed most of the glass-forming element Co and thus dramatically decreased the GFA of the alloy. Similar effect of Zr was observed, as shown in Fig. 12b. The addition of Zr induced formation of the black ternary $Al_{45}Zr_{45}Co_{10}$ phase, leading to a much reduced GFA. Therefore, phase competition and composition partitioning should be carefully controlled as far as addition of the elements with a positive heat of mixing with the main constituents is considered.

Methods

Master alloys were prepared by arc-melting a mixture of La and Ce (99.5%), Al and Cu (99.999%), Co (99.95%) and Fe (99.99%) in a Ti-gettered helium atmosphere. All the ingots were melted six times in order to ensure good chemical homogeneity. The rods with a different diameter ranging from 2 to 15 mm were prepared by casting the re-melt ingots into water-cooled copper molds under the helium atmosphere. Glass formation in the as-cast samples was mainly examined by X-ray diffraction (XRD) with Cu K_α radiation, scanning election microscopy (SEM) equipped with an EDX analyzer and high resolution transmission electron microscopy (HRTEM). The TEM samples were first mechanically ground to about 40 μm thick and then twin-jet electro-polished using a solution mixed in the ratio HClO4 : C2H6O = 1 : 19. Crystallization behavior of all as-prepared ingots and rods was studied by differential scanning calorimetry (DSC) at a heating rate of 20 K/min. The melting and solidification behavior of these alloys were characterized using differential thermal analysis (DTA) at a rate of 20 K/min.

1. Wu, Y., Xiao, Y. H., Chen, G. L., Liu, C. T. & Lu, Z. P. Bulk metallic glass composites with transformation-mediated work-hardening and ductility. *Adv. Mater.* **22**, 2770–2773 (2010).
2. Telford, M. The case for bulk metallic glass. *Mater. Today.* **7**, 36 (2004).
3. Inoue, A. Stabilization of metallic supercooled liquid and bulk amorphous alloys. *Acta. Mater.* **48**, 279–306 (2000).
4. Wu, Y. *et al.* Formation of Cu-Zr-Al bulk metallic glass composites with proved tensile properties. *Acta. Mater.* **59**, 2928–2936 (2011).
5. Pang, S. J., Zhang, T., Asami, K. & Inoue, A. Synthesis of Fe-Cr-Mo-C-B-P bulk metallic glasses with high corrosion resistance. *Acta. Mater.* **50**, 489–497 (2002).
6. Poon, S. J. & SHiflet, G. J. Synthesis and properties of metallic glasses that contain aluminum. *Science.* **241**, 1640–1642 (1988).
7. Lu, Z. P., Liu, C. T., Thompson, J. R. & Porter, W. D. Structural amorphous steels. *Phys. Rev. Lett.* **92**, 245503 (2004).
8. Schroers, J. Processing of bulk metallic glass. *Adv. Mater.* **22**, 1566–1597 (2010).
9. Inoue, A. & Wang, X. M. Bulk amorphous FC20 (Fe-C-Si) alloys with small amounts of B and their crystallized structure and mechanical properties. *Acta. Mater.* **48**, 1383–1395 (2000).
10. Inoue, A. Amorphous, nanoquasicrystalline and nanocrystalline alloys in Al-based systems. *Prog. Mater. Sci.* **43**, 365–520 (1998).
11. Inoue, A. & Kimura, H. Fabrications and mechanical properties of bulk amorphous, nanorcystalline, nanoquasicrystalline alloys in aluminum-based system. *J. Light. Met.* **1**, 31–41 (2001).
12. Yang, B. J. *et al.* Al-rich bulk metallic glasses with plasticity and ultrahigh specific strength. *Scripta. Mater.* **61**, 423–426 (2009).
13. Gu, X. J., Jin, H. J., Zhang, H. W., Wang, J. Q. & Lu, K. Pressure-enhanced thermal stability against eutectic crystallization in Al-based metallic glasses. *Scripta. Mater.* **45**, 1091–1097 (2001).
14. Chen, Z. P. *et al.* Role of rare-elements in glass formation of Al-Ca-Ni amorphous alloys. *J. Alloys. Compd.* **513**, 387–392 (2012).
15. Yang, H., Wang, J. Q. & Li, Y. Influence of TM and RE elements on glass formation of the ternary Al-TM-RE systems. *J. Non-Cryst. Solids.* **354**, 3473–3479 (2008).
16. Sanders, W. S., Warner, J. S. & Miracle, D. B. Stability of Al-rich glasses in the Al-La-Ni system. *Intermetallics.* **14**, 348–351 (2006).
17. Guo, F. Q., Enouf, S. J., Poon, S. J. & Shiflet, G. J. Formation of ductile Al-based metallic glasses without rare-earth elements. *Philos. Mag. Lett.* **81**, 203–211 (2001).
18. Sun, B. A. *et al.* Aluminum-rich bulk metallic glasses. *Scripta. Mater.* **59**, 1159–1162 (2008).
19. Poon, S. J., Shiflet, G. J., Guo, F. Q. & Ponnambalam, V. Glass formability of ferrous- and aluminum-based structural metallic alloys. *J. Non-cryst. Solids.* **317**, 1–9 (2003).
20. Miracle, D. B. A structural model for metallic glasses. *Nature. Mater.* **3**, 697–702 (2004).
21. Sheng, H. W., Luo, W. K., Alamgir, F. M., Bai, J. M. & Ma, E. Atomic packing and short-to-medium range order in metallic glasses. *Nature.* **439**, 419–425 (2006).
22. Angell, C. A. Formation of glasses from liquids and biopolymers. *Science.* **267**, 1924–1935 (1995).
23. Greer, A. L. Metallic glasses. *Science.* **267**, 1947–1953 (1995).
24. Wang, A. P., Wang, J. Q. & Ma, E. Modified efficient cluster packing model for calculating alloy compositions with high glass forming ability. *Appl. Phy. Lett.* **90**, 121912 (2007).
25. Senkov, O. K. & Miracle, D. B. Effect of the atomic size distribution on glass forming ability of amorphous metallic alloys. *Mater. Res. Bull.* **36**, 2183–2198 (2001).
26. Kim, Y. K., Soh, J. R., Kim, D. K. & Lee, H. M. Glass formation in metallic Al-Ni-Y. *J. Non-Cryst. Solids.* **242**, 122–130 (1998).
27. Greer, A. L. Confusion by design. *Nature.* **366**, 303–304 (1993).
28. Turnbull, D. Under what condition can a glass be formed. *Contemp. phys.* **10**, 473–488 (1969).
29. Lu, Z. P., Liu, C. T., Thompson, J. R. & Porter, W. D. Structural amorphous steels. *Phys. Rev. Lett.* **92**, 245503 (2004).
30. Lu, Z. P. & Liu, C. T. Glass formation criterion for various glass-forming systems. *Phys. Rev. Lett.* **91**, 115505 (2003).
31. Dougherty, G. M., Shiflet, G. J. & Poon, S. J. Synthesis and microstructural evolution of Al-Ni-Fe-Gd metallic glass by mechanical alloying. *Acta. Metall. Mater.* **42**, 2275–2283 (1994).

32. Wei, X. *et al*. Fabrication of Al-based bulk metallic glass by mechanical alloying and vacuum hot consolidation. *J. Alloys. Compd.* **501**, 164–167 (2010).
33. Choi, P. P. *et al*. Al-La-Ni-Fe bulk metallic glasses produced by mechanical alloying and spark-plasma sintering. *Mater. Sci. Eng. A.* **449–451**, 1119–1122 (2007).
34. Zhang, T., Li, R. & Pang, S. J. Effect of similar elements on improving glass-froming ability of La-Ce-based alloys. *J. Alloys Compd.* **483**, 60–63 (2009).
35. Li, R., Pang, S. J., Ma, C. L. & Zhang, T. Influence of similar atom substitution on glass formation in (La-Ce)-Al-Co bulk metallic glasses. *Acta. Mater.* **55**, 3719–3726 (2007).
36. Chen, D., Takeuchi, A. & Inoue, A. Gd-Co-Al and Gd-Ni-Al bulk metallic glasses with high glass forming ability and good mechanical properties. *Mater. Sci. Eng. A.* **457**, 226–230 (2007).
37. Lu, Z. P., Ma, D., Liu, C. T. & Chang, Y. A. Competitive formation of glasses and glass-matrix composites. *Intermetallics.* **253**, 253–259 (2007).
38. Baker, H. ASM Handbook, Volume 3: Alloy Phase Diagrams (ASM Handbook Committee, Ohio, Metals Park, 1992).
39. Takeuchi, A. & Inoue, A. Classification of bulk metallic glass by atomic size difference, heat of mixing and period of constituent elements and its application to characterization of the main alloying element. *Mater. Trans.* **12**, 2817–2829 (2005).

Acknowledgments

This research was supported in part by National Natural Science Foundation of China (No. 51010001 and 51001009), 111 Project (B07003) and Program for Changjiang Scholars and Innovative Research Team in University.

Author contributions

Z.P.C., Z.P.L. designed the research; Z.P.C., J.E.G. and Y.W. developed and characterized the alloy. H.W. carried out the mechanical testing; Z.P.C., X.J.L. and Z.P.L. wrote the manuscript.

Additional information

Competing financial interests: The authors declare no competing financial interests.

How to cite this article: Chen, Z.P. *et al*. Designing novel bulk metallic glass composites with a high aluminum content. *Sci. Rep.* **3**, 3353; DOI:10.1038/srep03353 (2013).